Published in final edited form as:

ACS Macro Lett. 2021 September 21; 10(9): 1151–1158. doi:10.1021/acsmacrolett.1c00500.

Motor-Driven Restructuring of Cytoskeleton Composites Leads to Tunable Time-Varying Elasticity

Janet Y. Sheung,
W. M. Keck Science Department, Scripps College, Pitzer College, and Claremont McKenna College, Claremont, California 91711, United States

Daisy H. Achiriloaie,
W. M. Keck Science Department, Scripps College, Pitzer College, and Claremont McKenna College, Claremont, California 91711, United States

Christopher Currie,
Department of Physics and Biophysics, University of San Diego, San Diego, California 92110, United States

Karthik Peddireddy,
Department of Physics and Biophysics, University of San Diego, San Diego, California 92110, United States

Aaron Xie,
W. M. Keck Science Department, Scripps College, Pitzer College, and Claremont McKenna College, Claremont, California 91711, United States

Jessalyn Simon-Parker,
W. M. Keck Science Department, Scripps College, Pitzer College, and Claremont McKenna College, Claremont, California 91711, United States

Gloria Lee,
Department of Physics and Biophysics, University of San Diego, San Diego, California 92110, United States

Corresponding Authors Janet Y. Sheung – jsheung@kecksci.claremont.edu, **Rae M. Robertson-Anderson** – randerson@sandiego.edu.

Author Contributions

R.M.R.-A. conceived the project, guided the experiments, interpreted the data, and wrote the manuscript. J.Y.S. designed, performed, and helped guide the experiments, analyzed and interpreted the data, and wrote the manuscript. D.H.A. helped perform experiments, analyzed data, prepared figures, and helped write the manuscript. C.C. analyzed data, prepared figures, and helped write the manuscript. A.X. helped analyze data and prepared figures. J.S.-P. prepared figures. K.P. helped guide experiments and analyzed and interpreted data. G.L. helped with materials preparation and data interpretation. M.J.R., M.D., and J.L.R. helped conceive the project and interpret data.

Notes

The authors declare no competing financial interest.

ASSOCIATED CONTENT

Supporting Information

The Supporting Information is available free of charge at https://pubs.acs.org/doi/10.1021/acsmacrolett.1c00500.

Section S1: Materials and Methods; Figure S1: confocal fluorescence images of microtubules in myosin-driven actin–microtubule composites show clustering and increased heterogeneity for hours after activation; Figure S2: data from Figure 2A plotted with log scaling on the *y*-axis (PDF)

Complete contact information is available at: https://pubs.acs.org/10.1021/acsmacrolett.1c00500

Michael J. Rust,
Department of Molecular Genetics and Cell Biology, University of Chicago, Chicago, Illinois 60637, United States

Moumita Das,
School of Physics and Astronomy, Rochester Institute of Technology, Rochester, New York 14623, United States

Jennifer L. Ross,
Department of Physics, Syracuse University, Syracuse, New York 13244, United States

Rae M. Robertson-Anderson
Department of Physics and Biophysics, University of San Diego, San Diego, California 92110, United States

Abstract

The composite cytoskeleton, comprising interacting networks of semiflexible actin and rigid microtubules, generates forces and restructures by using motor proteins such as myosins to enable key processes including cell motility and mitosis. Yet, how motor-driven activity alters the mechanics of cytoskeleton composites remains an open challenge. Here, we perform optical tweezers microrheology and confocal imaging of composites with varying actin–tubulin molar percentages (25–75, 50–50, and 75–25), driven by light-activated myosin II motors, to show that motor activity increases the elastic plateau modulus by over 2 orders of magnitude by active restructuring of both actin and microtubules that persists for hours after motor activation has ceased. Nonlinear microrheology measurements show that motor-driven restructuring increases the force response and stiffness and suppresses actin bending. The 50–50 composite exhibits the most dramatic mechanical response to motor activity due to the synergistic effects of added stiffness from the microtubules and sufficient motor substrate for pronounced activity.

Graphical Abstract

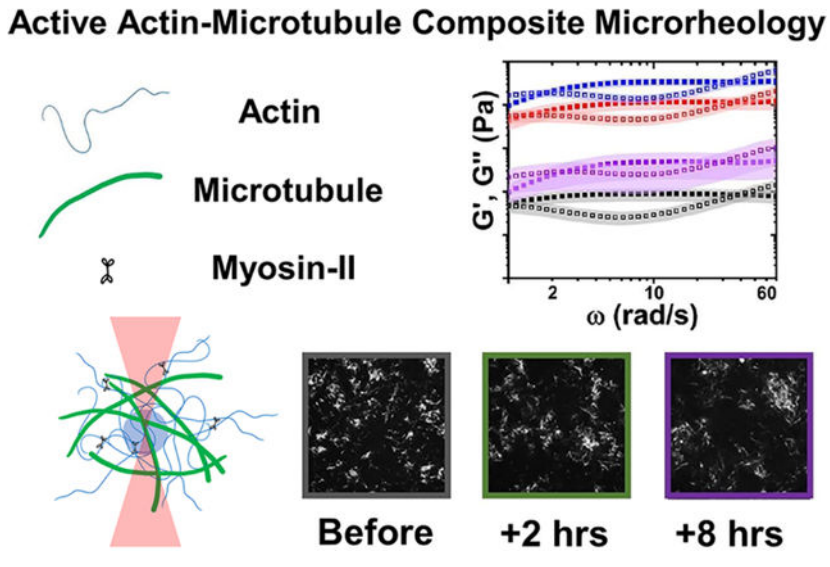

The cytoskeleton is an active composite of protein filaments capable of restructuring on demand to meet the wide variety of mechanical properties needed by eukaryotic cells, such as structural rigidity and malleability.[1–4] Semiflexible actin filaments, rigid microtubules, and intermediate filaments all contribute to this versatility by forming interacting viscoelastic networks.[2,5–8] In addition, molecular motors, such as actin-associated myosins, stochastically bind and actively pull on filaments, generating forces to contract and rearrange the cytoskeleton.[9–12] Motor-driven active dynamics play a critical role in enabling the cytoskeleton to rapidly tune its mechanical properties to achieve a myriad of different functions in response to environmental cues. At the same time, interactions between actin and microtubules play equally important roles in processes such as cell division, migration, and wound healing.[1,13–17] As such, the cytoskeleton is an exemplar of active matter that has been intensely studied not only for its biological relevance but also for its importance in the design of active nonequilibrium materials.[18,19,12,20,21] Nevertheless, the mechanical properties of the active composite cytoskeleton remain poorly understood.

Numerous in vitro studies have been performed on actomyosin systems, reporting a range of structural and dynamical properties depending on the concentrations of actin, myosin, and cross-linkers.[22,10,23,24,21,25] With sufficiently high cross-linker concentration, actomyosin activity induces large-scale contraction and coarsening of disordered actin networks.[26,22,27–29,24] However, at lower cross-linker densities, networks undergo destabilizing flow and rupturing into disconnected foci, thereby weakening the network.[22,27] We previously showed that incorporating microtubules into an actomyosin network provides a mechanical scaffold that enables controlled contractile dynamics, without flow or rupturing, in the absence of cross-linkers.[9] We also showed, surprisingly, that both actin and microtubules exhibited ballistic motion, with speeds that were indistinguishable from one another.[9,30] This result differs from that of steady-state composites of cross-linked actin and microtubules in which the mobilities of actin and microtubules were distinct.[22]

The rheology of actomyosin systems is far less understood, primarily due to the fact that microrheology methods typically used to investigate similar biological systems rely on the generalized Stokes–Einstein relation (GSER) to derive viscoelastic moduli from thermal fluctuations of embedded particles.[21] In nonequilibrium active systems, GSER is violated over frequency ranges comparable to those of motor-driven activity.[22] Previous attempts to investigate the mechanics of actomyosin systems have shown that particle fluctuations are dominated by motor activity at low frequencies while thermal fluctuations dominate the high-frequency regime.[23] However, how interactions between actin and microtubules impact the rheology of actomyosin systems remains completely unexplored.

We previously showed that the mechanics of steady-state actin–microtubule composites can be tuned by varying the relative concentrations of actin, microtubules, and cross-linkers.[22,27,31] Notably, we found that increasing microtubule concentration suppressed actin bending and led to more elastic-like response, while increasing actin concentration decreased mechanical heterogeneity by reinforcing microtubules against buckling.

Here, we perform linear and nonlinear optical tweezers microrheology to characterize the microscale force response of myosin-driven actin–microtubule composites before, during,

and following myosin activity (Figure 1 and Section S1). We circumvent GSER violation by performing measurements on judiciously tuned composites, with actin–tubulin molar percentages of 25–75, 50–50, and 75–25, which visibly restructure on the order of minutes yet are still slow enough ($\omega_{\text{active}} < 0.2$ rad/s) to be considered quasi-static (i.e., dominated by thermal fluctuations) for frequencies above approximately 1 rad/s. In addition, we use a light-sensitive myosin inhibitor, blebbistatin, to precisely control the location and duration of motor activity, enabling measurements before, during, and at precise time points after motor activity. We complement our measurements with confocal fluorescence imaging to show that the increased elasticity we measure, tuned by the molar percentages of actin and tubulin, results from mesoscale restructuring of homogeneous entangled meshes to more sparsely connected clusters and bundles.

To characterize the linear force response, we measure the force fluctuations (F_x, F_y) of optically trapped beads within the composites before, during, 4 h after, and 8 h after myosin activation (via blebbistatin deactivation) (Figure 1C and Figure S2). The magnitude of the fluctuations $|F(t)| = \left(F_x^2 + F_y^2\right)^{1/2}$ increases during and following myosin activity for all composites, with 50–50 exhibiting the most pronounced increase. Interestingly, while we see no visible signs of contraction on the order of minutes, after we halt activation, all composites continue to change their mechanical properties for at least 8 h following activation. In fact, in all cases, the maximum $|F(t)|$ was largest 4 h after motor activation ceased, rather than during active contraction (Figure S2). At this time, the force exerted on the trapped bead by the 50–50 composite increased beyond the strength of the trap in some cases as indicated by the arrows in Figure 2A.

From the force fluctuations we determine the frequency-dependent storage and loss moduli, $G'(\omega)$ and $G''(\omega)$, using GSER as previously described (Section S1, Figure 2C).[32–34] Because GSER is only strictly valid for steady-state thermal systems, we restrict our analyses to frequencies well above the active driving frequency ω_{active}, which we determine by using our previously measured contraction velocity $v \approx 35$ nm/s for the fastest composite (75 – 25).[30] We compute $\omega_{\text{active}} = 2\pi\dot{\gamma}_{\text{active}} \approx 0.18$ rad/s and thus safely approximate a quasi-steady state for $\omega > 1$ rad/s ($>5\omega_{\text{active}}$).[35]

As shown in Figure 2B, the viscoelastic moduli for all composites and time points exhibit strong entanglement behavior with the storage modulus $G'(\omega)$, a measure of elastic storage, exhibiting a plateau G_N^0, and $G''(\omega)$, the dissipative component, exhibiting a local minimum.[36] With motor activity, the magnitude of the elastic plateau G_N^0 increases by 1–2 orders of magnitude for all composites and continues to increase up to 4 h after activation, after which it drops but maintains a higher value compared to preactivation. This drop at 8 h is most dramatic for 50–50 while nearly undetectable for 75–25. As G_N^0 is predicted to scale linearly with the number of entanglements along each polymer, this nonmonotonic dependence of G_N^0 on time, relative to motor activation, signifies a substantial increase in entanglement density followed by relaxation back to a less densely entangled mesh.[36]

Nearly all composites exhibit crossovers of $G'(\omega)$ and $G''(\omega)$ at both low and high frequencies (Figure 2B). For entangled polymers, the high crossover frequency, ω_{c1}, is a measure of the entanglement time τ_e, i.e., the time at which filament–filament interactions become important,[28] while the low crossover frequency, ω_{c2}, is a measure of the tube model disengagement time τ_D, i.e., the time at which filaments curvilinearly diffuse out of their confinement tubes. We measure $\tau_{c1} = \frac{2\pi}{\omega_{c1}}$ values of ~0.14–0.24 s, comparable to the predicted entanglement time of ~0.25 s for an actin network at the same concentration.[37,38] As previously shown and predicted,[37,20] the lower values we measure after activity are likely due to actin bundling which decreases τ_{c1} as bundles become stiffer and more connected.

We measure $\tau_{c2} = \frac{2\pi}{\omega_{c2}}$ values of ~4–9 s for all composites, quite similar to the previously reported longest relaxation times of ~3–9 s for comparable actin–microtubule composites that lacked motors.[27] As in this previous work, we attribute the relatively fast disengagement time, compared to predictions,[37,38] as arising from entanglement hopping, whereby filaments can periodically move transversely to their contours due to temporary release of an entanglement with a neighboring filament.[31,38,39] We note that τ_{c2} generally decreases (albeit with substantial noise) for all composites during and following activation, which may arise from more hopping events as the network restructures, releasing and reforming entanglements.

To determine the extent to which motor-driven viscoelastic changes are preserved when the composite is driven far from steady state, we perform nonlinear constant-rate strain measurements before and 2 h after motor activation. Specifically, we measure the force exerted on an optically trapped bead as we displace it at a constant speed and subsequently hold it fixed to measure the force relaxation (Figure 1D). We also attempted this protocol at 4 h after activation, but the 50–50 composite was too stiff to complete most of the measurements without the bead being pulled out of the trap, consistent with the continued increase in G_N^0 (Figure 2).

As shown in Figure 3A, the force response both before and after activity is solid-like (i.e., linear strain dependence) over the entire strain for all composites, but the force magnitudes and slopes all increase after activity. While the maximum force increases by >2× for 50–50 and 75–25, with 50–50 exhibiting the highest resistive force, it only modestly increases for 25–75. In all composites, the increase is a lower bound that does not include the trials in which the trapping force could not withstand the composite force (indicated by single data points in Figure 3A). To quantify the increased slope, a measure of composite stiffness, we compute the strain-averaged differential modulus $K = \mathrm{d}F/\mathrm{d}x$ (Figure 3A, inset). As shown, K values follow a similar trend as the force magnitude, suggestive of more bundled filaments that are stiffer and more readily resist strain.

The force relaxation curves following strain (Figure 3B,C) show that both before and 2 h after activation all composites maintain some degree of strain memory (i.e., nonzero force) at the end of the relaxation phase. However, this nonzero terminal force F_∞, a signature of solid-like mechanics, is >2× higher following myosin activation for all composites, in line

with our previous measurements on statically cross-linked actin–microtubule composites (Figure 3B).[22,27] Notably, while the force during strain for 25–75 does not increase significantly after motor activity, the stress–relaxation is markedly suppressed. Considering F_∞, we find that nearly all relaxations fit well to a sum of two exponentials with well-separated time constants: $F(t) = F_\infty + C_1 e^{-t/\tau 1} + C_2 e^{-t/\tau 2}$. We interpret each decay as arising from a distinct relaxation mechanism with a characteristic decay time τ_i and a relative contribution to the stress–relaxation $c_i = C_i/(C_1 + C_2)$ (Figure 3C,D). The exception is 25–75 after activity, which is accurately described by a single exponential that lacks the fast time scale τ_1.

Our slow relaxation time scales are similar to our measured τ_{C_2} values before and after activity for all composites (Figure 2E) and likewise modestly decrease following motor activity. As such, we understand this time scale as arising from reptation and hopping, facilitated by restructuring.[31] To understand our fast relaxation time scale, τ_1, we evaluate the predicted actin bending time scale, $\tau_B \approx \gamma L/(l_p k_b T(3\pi/2)^4)$, where $L \approx 8.7 \pm 2.8$ μm is the average actin filament length,[31,38,39] $l_p \approx 17$ μm the persistence length,[40] and $\gamma = 4\pi\eta/\ln(2\xi/r)$ the drag coefficient, with η the solvent viscosity, $\xi \approx 0.85$ μm the actin mesh size,[41] and $r \approx 3$ nm the filament radius.[42] Our computed value $\tau_B \approx 0.54 \pm 0.17$ s (shown as dashed line in Figure 3C) is quite close to our measured fast time scales (Figure 3C).

By evaluating the relative contribution of each relaxation mechanism (c_1, c_2) before and after activity (Figure 3C), we find that in all cases the slow mode contributes more to the relaxation than the fast mode ($c_2 > c_1$). Following motor activation, the fast bending contribution decreases further, or is eliminated, and c_2 concomitantly increases. Motor activity may suppress bending by bundling filaments, reducing their susceptibility to thermal bending.[43] The lack of τ_1 in 25–75 suggests that actin bundling, along with the larger percentage of microtubules, is sufficient to suppress bending entirely. Notably, these results are distinct from our results for statically cross-linked composites, in which the fast mode contributed >2× more than the slow mode, even with substantial crosslinking.[22]

We hypothesize that the rheological behavior shown in Figures 2 and 3 is due to restructuring of composites from meshes of individual filaments to networks of bundles and clusters.[37,44,45] To test this hypothesis, we analyze confocal fluorescence images of rhodamine-labeled microtubules in composites at the same time points that we perform microrheology (Figure 4 and Figure S1).

The images show clear restructuring of all composites over 8 h following myosin activation (Figure 4A), which we quantify by computing the spatial image autocorrelation function $g(r)$ (see Section S1), which determines the degree to which the intensity at one location in an image correlates with the intensity of the surrounding points at varying distances.[46] The slower $g(r)$ decays with increasing r, the larger the structural features of the network. Average $g(r)$ curves exhibit clear broadening over time after motor activation, as shown for 50–50 in Figure 4B, suggesting formation of clusters separated by larger, sparsely populated gaps. By fitting $g(r)$ to an exponential $g(r) = Ae^{-r/\xi}$, we determine a characteristic decay length or correlation length ξ, which scales as the mesh size for an isotropic network.[47] As

shown in Figure 4C, the magnitude and spread of ξ values increase with time following activation for all composites, consistent with the restructuring we describe above.

Importantly, the mechanical properties we report here are distinct from those expected for actomyosin networks without microtubules. Namely, in actomyosin networks without cross-linkers, motor activity causes network rupturing and fluidization. Such activity would result in reduced elasticity as well as unstable structure following activity. Here, microtubules act as a scaffold that reinforces and further connects the actin, allowing myosin to contract the network into clusters while maintaining connectivity and mechanical integrity over extended periods and when subject to nonlinear forcing.[9]

In addition, we show that the 50–50 composite surprisingly exhibits the highest strength and elasticity (rather than 25–75 that has more rigid microtubules) as well as the strongest effect of motor activity (rather than 75–25 that has more actin for myosin to act on). While composites with more actin (75–25) have more active substrate, they are inherently floppier and require more contraction to achieve the same stiffness and rigidity that 50–50 confers. Likewise, 25–75 is stiffer from the outset but has less active substrate, so is less susceptible to motor-driven restructuring.

In summary, we couple optical tweezers microrheology with fluorescence confocal microscopy to elucidate the effects of myosin II activity on the mechanics and structure of entangled actin–microtubule composites. We show that motor activity increases the plateau modulus, resilience to nonlinear straining, and mechano-memory and suppresses filament bending during motor activity and for hours after cessation of motor activation. This time-varying mechanical response is due to slow restructuring from an entangled mesh of individual filaments to a network of dense bundles. Our results provide valuable insight into the mechanics of active cytoskeletal systems and how the interplay between motor activity, the composite nature of the cytoskeleton, and time-varying structure leads to the myriad mechanical properties that cells exhibit. More generally, our techniques and results can be applied to a wide range of active matter systems currently under intense investigation.

EXPERIMENTAL SECTION

Many of the materials and methods are described in the main text and in the captions of Figures 1–4. More detailed descriptions of all materials and methods are included in Section S1 of the Supporting Information.

Supplementary Material

Refer to Web version on PubMed Central for supplementary material.

ACKNOWLEDGMENTS

This research was funded by a William M. Keck Foundation Research Grant and a National Institute of General Medical Sciences Award (no. R15GM123420). J.Y.S. acknowledges startup support from the W. M. Keck Science Department of Claremont McKenna, Scripps, and Pitzer Colleges of The Claremont Colleges. The authors are grateful to Jonathan Garamella and Ryan McGorty for helpful discussions and to Gregor Leech and Ryan Clairmont for assistance in instrument calibrations.

REFERENCES

(1). Burla F; Mulla Y; Vos B; Aufderhorst-Roberts A; Koenderink G From Mechanical Resilience to Active Material Properties in Biopolymer Networks. Nat. Rev. Phys. 2019, 1, 249.

(2). Fletcher DA; Mullins RD Cell Mechanics and the Cytoskeleton. Nature 2010, 463 (7280), 485–492. [PubMed: 20110992]

(3). Forth S; Kapoor TM The Mechanics of Microtubule Networks in Cell Division. J. Cell Biol. 2017, 216 (6), 1525–1531. [PubMed: 28490474]

(4). Barlan K; Gelfand VI Microtubule-Based Transport and the Distribution, Tethering, and Organization of Organelles. Cold Spring Harbor Perspect. Biol 2017, 9 (5), a025817.

(5). Blanchoin L; Boujemaa-Paterski R; Sykes C; Plastino J Actin Dynamics, Architecture, and Mechanics in Cell Motility. Physiol. Rev. 2014, 94 (1), 235–263. [PubMed: 24382887]

(6). Gruenbaum Y; Aebi U Intermediate Filaments: A Dynamic Network That Controls Cell Mechanics. F1000Prime Rep. 2014, 6, 54. [PubMed: 25184044]

(7). Helfand BT; Mikami A; Vallee RB; Goldman RD A Requirement for Cytoplasmic Dynein and Dynactin in Intermediate Filament Network Assembly and Organization. J. Cell Biol. 2002, 157 (5), 795–806. [PubMed: 12034772]

(8). Schliwa M; van Blerkom J Structural Interaction of Cytoskeletal Components. J. Cell Biol. 1981, 90 (1), 222–235. [PubMed: 7019221]

(9). Lee G; Leech G; Rust MJ; Das M; McGorty RJ; Ross JL; Robertson-Anderson RM Myosin-Driven Actin-Microtubule Networks Exhibit Self-Organized Contractile Dynamics. Sci. Adv. 2021, 7 (6), No. eabe4334. [PubMed: 33547082]

(10). Köster DV; Husain K; Iljazi E; Bhat A; Bieling P; Mullins RD; Rao M; Mayor S Actomyosin Dynamics Drive Local Membrane Component Organization in an in Vitro Active Composite Layer. Proc. Natl. Acad. Sci. U. S. A. 2016, 113 (12), E1645–E1654. [PubMed: 26929326]

(11). Ideses Y; Sonn-Segev A; Roichman Y; Bernheim-Groswasser A Myosin II Does It All: Assembly, Remodeling, and Disassembly of Actin Networks Are Governed by Myosin II Activity. Soft Matter 2013, 9 (29), 7127–7137.

(12). Needleman D; Dogic Z Active Matter at the Interface between Materials Science and Cell Biology. Nat. Rev. Mater. 2017, 2 (9), 1–14.

(13). Dogterom M; Koenderink GH Actin–Microtubule Crosstalk in Cell Biology. Nat. Rev. Mol. Cell Biol. 2019, 20 (1), 38–54. [PubMed: 30323238]

(14). Vertii A; Hehnly H; Doxsey S The Centrosome, a Multitalented Renaissance Organelle. Cold Spring Harbor Perspect. Biol 2016, 8 (12), a025049.

(15). Saltini M; Mulder BM Microtubule-Based Actin Transport and Localization in a Spherical Cell. R. Soc. Open Sci. 2020, 7 (11), 201730. [PubMed: 33391819]

(16). Colin A; Singaravelu P; Théry M; Blanchoin L; Gueroui Z Actin-Network Architecture Regulates Microtubule Dynamics. Curr. Biol. 2018, 28 (16), 2647–2656. [PubMed: 30100343]

(17). Stossel TP On the Crawling of Animal Cells. Science 1993, 260 (5111), 1086–1094. [PubMed: 8493552]

(18). Gagnon DA; Dessi C; Berezney JP; Boros R; Chen DT-N; Dogic Z; Blair DL Shear-Induced Gelation of Self-Yielding Active Networks. Phys. Rev. Lett. 2020, 125 (17), 178003. [PubMed: 33156652]

(19). Farhadi L; Fermino Do Rosario C; Debold EP; Baskaran A; Ross JL Active Self-Organization of Actin-Microtubule Composite Self-Propelled Rods. Front. Phys. 2018, DOI: 10.3389/fphy.2018.00075.

(20). Sanchez T; Chen DTN; DeCamp SJ; Heymann M; Dogic Z Spontaneous Motion in Hierarchically Assembled Active Matter. Nature 2012, 491 (7424), 431–434. [PubMed: 23135402]

(21). Koenderink GH; Dogic Z; Nakamura F; Bendix PM; MacKintosh FC; Hartwig JH; Stossel TP; Weitz DA An Active Biopolymer Network Controlled by Molecular Motors. Proc. Natl. Acad. Sci. U. S. A. 2009, 106 (36), 15192–15197. [PubMed: 19667200]

(22). Francis ML; Ricketts SN; Farhadi L; Rust MJ; Das M; Ross JL; Robertson-Anderson RM Non-Monotonic Dependence of Stiffness on Actin Crosslinking in Cytoskeleton Composites. Soft Matter 2019, 15 (44), 9056–9065. [PubMed: 31647488]

(23). Murrell MP; Gardel ML F-Actin Buckling Coordinates Contractility and Severing in a Biomimetic Actomyosin Cortex. Proc. Natl. Acad. Sci. U. S. A. 2012, 109 (51), 20820–20825. [PubMed: 23213249]

(24). Silva M. S. e.; Depken M; Stuhrmann B; Korsten M; MacKintosh FC; Koenderink GH Active Multistage Coarsening of Actin Networks Driven by Myosin Motors. Proc. Natl. Acad. Sci. U. S. A. 2011, 108 (23), 9408–9413. [PubMed: 21593409]

(25). Storm C; Pastore JJ; MacKintosh FC; Lubensky TC; Janmey PA Nonlinear Elasticity in Biological Gels. Nature 2005, 435 (7039), 191–194. [PubMed: 15889088]

(26). Fürthauer S; Lemma B; Foster PJ; Ems-McClung SC; Yu C-H; Walczak CE; Dogic Z; Needleman DJ; Shelley MJ Self-Straining of Actively Crosslinked Microtubule Networks. Nat. Phys. 2019, 15 (12), 1295–1300. [PubMed: 32322291]

(27). Ricketts SN; Francis ML; Farhadi L; Rust MJ; Das M; Ross JL; Robertson-Anderson RM Varying Crosslinking Motifs Drive the Mesoscale Mechanics of Actin-Microtubule Composites. Sci. Rep. 2019, 9 (1), 12831. [PubMed: 31492892]

(28). Lenz M Geometrical Origins of Contractility in Disordered Actomyosin Networks. Phys. Rev. X 2014, 4 (4), 041002.

(29). Yang Y; Bai M; Klug WS; Levine AJ; Valentine MT Microrheology of Highly Crosslinked Microtubule Networks Is Dominated by Force-Induced Crosslinker Unbinding. Soft Matter 2013, 9 (2), 383–393. [PubMed: 23577042]

(30). Lee G; Leech G; Lwin P; Michel J; Currie C; Rust MJ; Ross JL; McGorty RJ; Das M; Robertson-Anderson RM Active Cytoskeletal Composites Display Emergent Tunable Contractility and Restructuring. bioRxiv 2021,.

(31). Ricketts SN; Ross JL; Robertson-Anderson RM Co-Entangled Actin-Microtubule Composites Exhibit Tunable Stiffness and Power-Law Stress Relaxation. Biophys. J. 2018, 115 (6), 1055–1067. [PubMed: 30177441]

(32). Tassieri M; Evans RML; Warren RL; Bailey NJ; Cooper JM Microrheology with Optical Tweezers: Data Analysis. New J. Phys. 2012, 14 (11), 115032.

(33). Evans RML; Tassieri M; Auhl D; Waigh TA Direct Conversion of Rheological Compliance Measurements into Storage and Loss Moduli. Phys. Rev. E 2009, 80 (1), 012501.

(34). Squires TM Nonlinear Microrheology: Bulk Stresses versus Direct Interactions. Langmuir 2008, 24 (4), 1147–1159. [PubMed: 18154310]

(35). Peddireddy KR; Lee M; Schroeder CM; Robertson-Anderson RM Viscoelastic Properties of Ring-Linear DNA Blends Exhibit Nonmonotonic Dependence on Blend Composition. Phys. Rev. Res. 2020, 2 (2), 023213.

(36). Doi M; Edwards SF The Theory of Polymer Dynamics; Clarendon Press: Oxford, 1988.

(37). Gurmessa B; Francis M; Rust MJ; Das M; Ross JL; Robertson-Anderson RM Counterion Crossbridges Enable Robust Multiscale Elasticity in Actin Networks. Phys. Rev. Res. 2019, 1 (1), 013016.

(38). Isambert H; Maggs AC Dynamics and Rheology of Actin Solutions. Macromolecules 1996, 29 (3), 1036–1040.

(39). Hinner B; Tempel M; Sackmann E; Kroy K; Frey E Entanglement, Elasticity and Viscous Relaxation of Actin Solutions. Phys. Rev. Lett. 1998, 81 (12), 2614–2617.

(40). Gittes F Flexural rigidity of microtubules and actin filaments measured from thermal fluctuations in shape. J. Cell Biol; https://rupress.org/jcb/article/120/4/923/28578/Flexural-rigidity-of-microtubules-and-actin (accessed 2021-04-24).

(41). Falzone TT; Blair S; Robertson-Anderson RM Entangled F-Actin Displays a Unique Crossover to Microscale Nonlinearity Dominated by Entanglement Segment Dynamics. Soft Matter 2015, 11 (22), 4418–4423. [PubMed: 25920523]

(42). Alberts B Molecular Biology of the Cell; Garland Science: 2017.

(43). MacKintosh FC; Levine AJ Nonequilibrium Mechanics and Dynamics of Motor-Activated Gels. Phys. Rev. Lett. 2008, 100 (1), 018104. [PubMed: 18232824]

(44). Lee H; Ferrer JM; Nakamura F; Lang MJ; Kamm RD Passive and Active Microrheology for Cross-Linked F-Actin Networks in Vitro. Acta Biomater. 2010, 6 (4), 1207–1218. [PubMed: 19883801]

(45). Shin JH; Gardel ML; Mahadevan L; Matsudaira P; Weitz DA Relating Microstructure to Rheology of a Bundled and Cross-Linked F-Actin Network in Vitro. Proc. Natl. Acad. Sci. U. S. A. 2004, 101 (26), 9636–9641. [PubMed: 15210969]

(46). Robertson C; M.d SCG Theory and Practical Recommendations for Autocorrelation-Based Image Correlation Spectroscopy. J. Biomed. Opt. 2012, 17 (8), 080801. [PubMed: 23224160]

(47). Sonn-Segev A; Bernheim-Groswasser A; Roichman Y Extracting the Dynamic Correlation Length of Actin Networks from Microrheology Experiments. Soft Matter 2014, 10 (41), 8324–8329. [PubMed: 25192175]

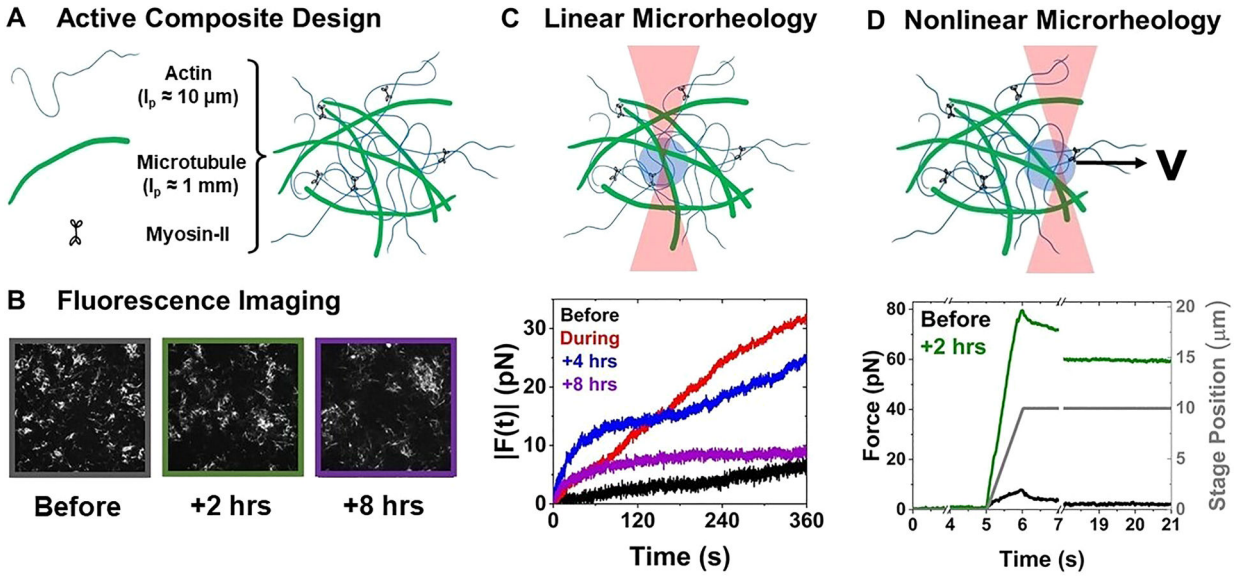

Figure 1.

Optical tweezers microrheology characterizes how actomyosin activity alters the mechanical response of actin–microtubule composites. (A) Cartoon of composite composed of actin filaments, microtubules, and myosin II minifilaments, prepared as described in the Supporting Information. (B) 512 pixel × 512 pixel (213 μm × 213 μm) fluorescence confocal images of rhodamine-labeled microtubules in a 50–50 actin–tubulin composite acquired before, 2 h after, and 8 h after myosin activation. (C) Linear microrheology. (top) Cartoon depicting trapping a 4.5 μm diameter microsphere within a composite and tracking its force fluctuations (F_x, F_y) for 3 min. (bottom) Sample force magnitudes $|F(t)| = \left(F_x^2 + F_y^2\right)^{1/2}$ measured for the 50–50 composite before (black), during (red), and 4 h (blue) and 8 h (purple) after myosin activation. (D) Nonlinear microrheology. (top) Cartoon of measurement in which we hold an optically trapped bead fixed for 5 s, displace the bead 5 μm through the composite at 5 μm/s, and then hold it fixed again for the remaining of the 20 s measurement. We measure the force exerted on the microsphere for the duration of the measurement. Example force measurement for the 50–50 composite before (black) and 2 h after (green) 10 min of myosin activation. The gray curve shows the position of the piezoelectric stage that displaces the bead relative to the composite.

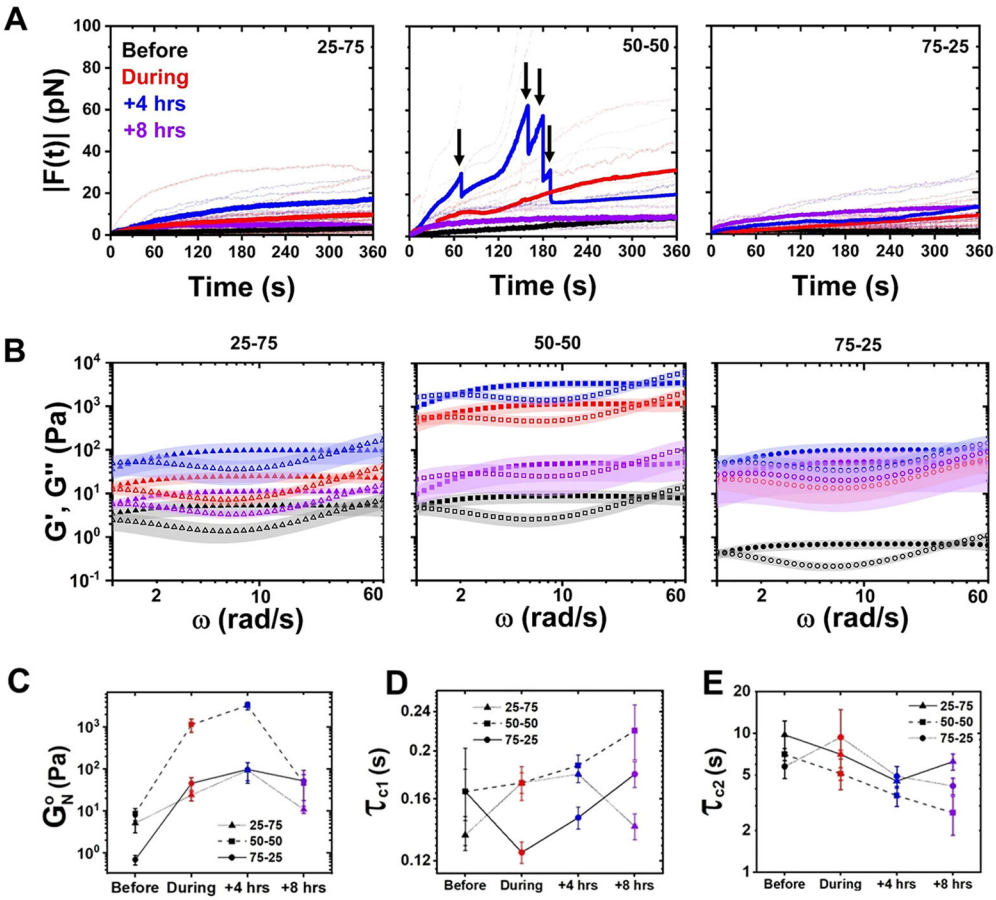

Figure 2.

Myosin activity universally increases the elastic plateau of actin–microtubule composites with varying compositions. (A) Magnitude of the force exerted on optically trapped microspheres, $|F(t)| = \left(F_x^2 + F_y^2\right)^{1/2}$, embedded in composites of varying actin–tubulin molar percentages (listed in each panel) measured before (black) and during (red) 3 min of myosin activation as well as 4 h (blue) and 8 h (purple) after. Lighter dotted lines indicate individual trials, and darker solid lines indicate averages of the individual trials shown. The force exerted by the 50–50 composite at +4 h exceeded the strength of the optical trap for some trials, leading to the truncated force curves shown in the 50–50 plot. Arrows above the average force curve during activity indicate locations where the number of individual trials contributing to the average decreases due to truncated trials. (B) Elastic ($G'(\omega)$, closed symbols) and viscous ($G''(\omega)$, open symbols) moduli computed from the forces shown in (A). Color coding and panel organization is as in (A). The shaded region surrounding each curve indicates standard error. (C) Elastic plateau modulus G_N^0 determined from the data shown in (B). (D, E) Fast (τ_{c1}, D) and slow (τ_{c2}, E) relaxation times determined from the high (ω_{c1}) and low (ω_{c2}) frequencies at which $G'(\omega)$ and $G''(\omega)$ cross.

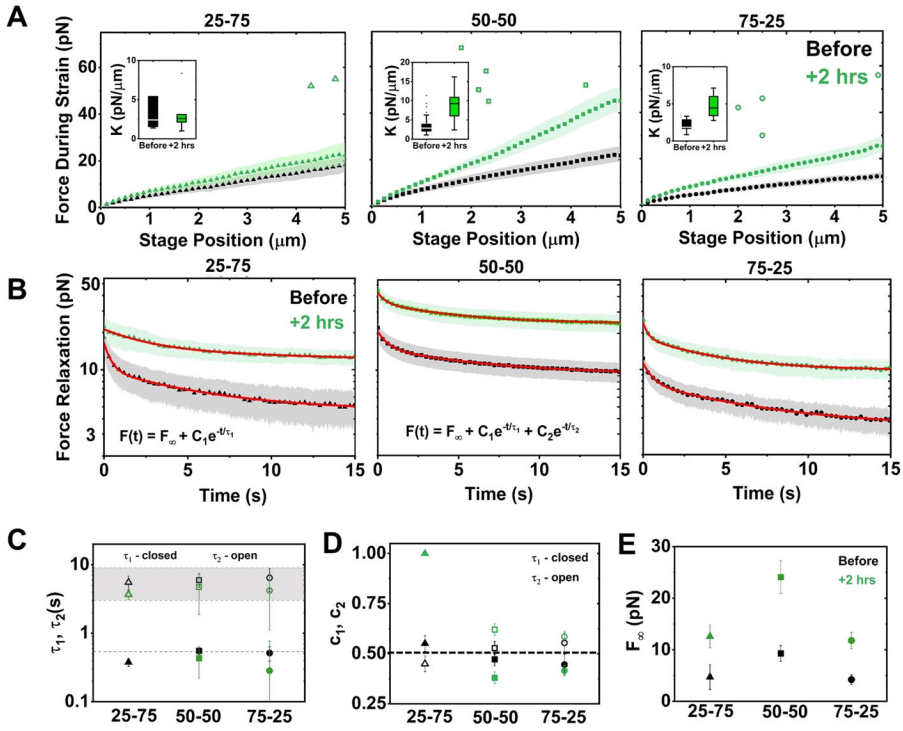

Figure 3.

Myosin-driven restructuring increases the nonlinear force response and suppresses relaxation of actin–microtubule composites. (A) Average force $F(x)$ exerted on the bead during nonlinear strain, measured before (black) and 2 h after (green) myosin activation, for composites with actin–tubulin percentages of 25–75 (left), 50–50 (middle), and 75–25 (right). Shaded regions along each curve indicate standard error. Insets: boxplots of differential modulus, $K = \mathrm{d}F/\mathrm{d}x$, found as the slope of $F(x)$ for each trial. (B) Relaxation of force versus time following strain, measured before and 2 h after motor activation. Nearly all curves are well fit to a sum of two exponentials and a nonzero offset: $F(t) = F_\infty + C_1 e^{-t/\tau 1} + C_2 e^{-t/\tau 2}$. The 25–75 relaxation after activation fits to a single exponential. Fits are shown as red lines. (C) Time constants corresponding to fast (τ_1, closed symbols) and slow (τ_2, open symbols) modes determined from fits in (B) for relaxations measured before (black) and 2 h after (green) activation. The dashed line corresponds to predicted actin bending time scale τ_B, and the gray region corresponds to previously measured reptation times for steady-state composites. (D) Relative contributions of the fast (c_1) and slow (c_2) modes determined from the fits in (B). Dashed horizontal line indicates equal contribution from both modes. (E) F_∞ determined from the fits shown in (B), corresponding to the force that is sustained at the end of the relaxation period.

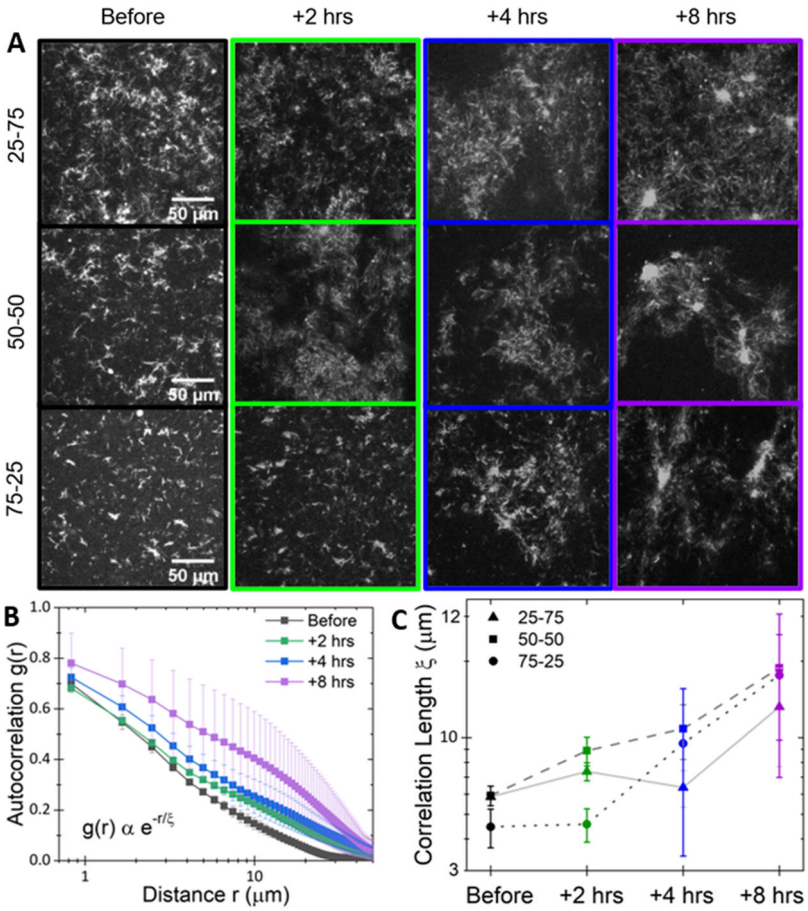

Figure 4.

Myosin activity drives sustained mesoscale clustering in actin–microtubule composites. (A) Representative 512 pixel × 512 pixel fluorescence confocal micrographs of rhodamine-labeled microtubules in actin–microtubule composites with actin–tubulin molar percentages of 25–75 (top), 50–50 (middle), and 75–25 (right). Images were acquired with 568 nm illumination at varying times relative to myosin activation: before (black) and 2 h (green), 4 h (blue), and 8 h (purple) after. (B) Average autocorrelation curves $g(r)$, computed from five images for each time point, for the 50–50 composite. Error bars are standard error. Curves are fit to the equation shown to determine the correlation length ξ for each composite and time shown in panel C. (C) Average correlation lengths ξ for 25–75 (triangles), 50–50 (squares), and 75–25 (circles) composites at each time shown in (A).